

Document downloaded from:

<http://hdl.handle.net/10251/140967>

This paper must be cited as:

Stoeger, JA.; Veziri, CM.; Palomino Roca, M.; Corma Canós, A.; Kanellopoulos, NK.; Tsapatsis, M.; Karanikolos, GN. (2012). On stability and performance of highly c-oriented columnar AlPO₄-5 and CoAPO-5 membranes. *Microporous and Mesoporous Materials*. 147(1):286-294. <https://doi.org/10.1016/j.micromeso.2011.06.028>



The final publication is available at

<https://doi.org/10.1016/j.micromeso.2011.06.028>

Copyright ELSEVIER SCIENCE BV

Additional Information

On Stability and Performance of Highly *c*-Oriented Columnar AlPO₄-5 and CoAPO-5 Membranes

Jared A. Stoeger¹, Charitomeni M. Veziri², Miguel Palomino³, Avelino Corma³, Nick K. Kanellopoulos², Michael Tsapatsis¹, Georgios N. Karanikolos^{2*}

1. Department of Chemical Engineering and Materials Science, University of Minnesota-Twin Cities, 421 Washington Avenue SE, Minneapolis, MN 55455 USA

2. Institute of Physical Chemistry, Demokritos National Research Center, Athens 153 10, Greece

3. Instituto de Tecnologia Quimica (CSIC-UPV), Universidad Politecnica de Valencia, Avda de los Naranjos s/n, 46022 Valencia, Spain

Corresponding Author:

Dr. Georgios N. Karanikolos

E-mail: karanikolos@chem.demokritos.gr

Abstract

Continuous films comprised of highly *c*-oriented aluminophosphate $\text{AlPO}_4\text{-5}$ or cobalt-substituted $\text{AlPO}_4\text{-5}$ (CoAPO-5) were grown on porous supports and subjected to heat treatment in order to investigate the potential for membrane applications. A study in the early stages of in-plane crystalline intergrowth revealed a potential mechanism for flake-like crystal formation between the original oriented columnar crystals. Variations in metal substitution ($\text{AlPO}_4\text{-5}$, CoAPO-5), support (glass, silicon, porous alumina) and calcination method (conventional, rapid thermal processing) were chosen to examine the conditions by which structural integrity was compromised following secondary (or tertiary) growth, resulting in reduced membrane functionality. Through the use of rapid thermal processing, the structure debilitation could be partially avoided. The membrane quality was inspected through pervaporation measurements consisting of a liquid hydrocarbon feed of n-heptane and 1,3,5-triisopropylbenzene. By investigating the effect of template removal on the oriented, columnar crystalline structure, useful insight is provided into the potential for the membranes to participate in applications such as molecular separations, catalysis, or host-guest assemblies.

Keywords: $\text{AlPO}_4\text{-5}$; CoAPO-5 ; membrane; oriented growth; rapid thermal processing; pervaporation.

1. Introduction

Since the inception of supported crystal growth, extensive research efforts have focused on fabricating high-quality films with control over microstructure characteristics such as continuity in coverage, a high degree of intergrowth, and a reduction in debilitating defects [1-3]. For instance, to be useful in molecular separations applications, the film would preferably allow fast component fluxes with high separation factors, so maintaining a thin, defect-free layer which could withstand high temperatures and pressures or harsh environments would prove to be influential to the commercialization of such technologies.

One-dimensional aluminophosphate AFI structure type ($\text{AlPO}_4\text{-5}$) materials have been theorized to compete alongside well-studied multi-dimensional systems of silicate and aluminosilicate based on the potential for fast mass transport by single file diffusion through the crystalline channels [4,5]. $\text{AlPO}_4\text{-5}$ has routinely been chosen for aluminophosphate film growth due to the unique system of parallel channels, down the length of the elongated c -axis of the hexagonal crystal lattice with 0.73 nm diameter cylindrical pore openings. Supported oriented growth of the aluminophosphate AFI type has been reported by a variety of techniques: using surface-modified gold substrates [6], in situ hydrothermal growth on stainless steel supports [7], electric field seed crystal alignment on glass [8], laser ablation on coated silicon wafers [9], epitaxial growth from specific crystal basal faces [10], microwave growth on anodic alumina [11,12], manual assembly on various PVA-coated substrates [13], and in situ growth on bare porous α - Al_2O_3 supports [14] or pre-coated with a thin chitosan layer [15]. We demonstrated an ability to control AFI film microstructure through seeded secondary and tertiary growth techniques on functionalized silicon substrates [16-18]. Realization of sub-micron thick,

continuous, oriented, intergrown AFI films was accomplished through modification of various seeding and growth parameters.

In addition to extending our proven microstructure control to porous supports, for AlPO_4 -5 and CoAPO-5 films to be useful for separation applications the structure directing agent (SDA) molecules occluded in the pore channels must be removed to allow for mass transport. The thermal behavior of aluminophosphate materials has varied. As mentioned, there have been significant investigations into fabricating high-quality oriented AlPO_4 -5 films, but few have published results following template removal [4,14]. While densified aluminophosphate forms have been reported following synthetic conditions intended to ensure crystalline microporous structures in the powder form [19], there have been numerous reports of post-synthetic heat treatment inducing framework destruction. In a report from Schnabel et al., decomposition of SDA molecules in SAPO-5 (Si-substituted AFI) and AlPO_4 -5 above 700 °C resulted in structural transformation to an aluminophosphate form of cristobalite [20]. Furthermore, Hu et al. studied several microporous aluminophosphates as well as dense aluminophosphate frameworks (tridymite, cristobalite) which are isostructural to similar forms composed of SiO_2 units [21]. Additionally, calcination of mesoporous aluminophosphate structures has been reported to yield densified forms (cristobalite, tridymite) with a concurrent pore structure loss [22], requiring solvent extraction and further calcination for even marginal thermal stability [23]. At temperatures up to 550 °C, cobalt-modified frameworks have resulted in total structure collapse to an amorphous form [24]. A study conducted by Lohse et al. determined that the thermal stability of CoAPO-5 samples decreases strongly as a function of the cobalt content, with temperatures as low as 200 °C inducing the formation of an AlPO_4 -tridymite

phase [25]. A similar phase has also been reported for vanadium-substituted $\text{AlPO}_4\text{-5}$ structures [26]. Additionally, in the years following its discovery, the large-pore, similarly one-dimensional aluminophosphate VPI-5 (VFI structure type, 1.27 nm pore channel diameter) was reported to be thermally unstable at elevated temperatures, transforming into $\text{AlPO}_4\text{-8}$ (AET structure type) with a rearrangement of framework atoms [27-29].

In the present work, we have attempted to study the structural stability of $\text{AlPO}_4\text{-5}$ films at temperatures necessary to remove occluded SDA molecules. By extending our knowledge of seeded secondary growth to porous $\alpha\text{-Al}_2\text{O}_3$ supports, we have analyzed the membrane functionality of columnar, highly *c*-oriented $\text{AlPO}_4\text{-5}$ and CoAPO-5 films for applications in molecular separations. It was discovered that intergrown, ordered supported columnar crystals of the AFI-framework type transformed to densified aluminophosphate tridymite at elevated temperatures, while the unsupported powder retained the AFI structure following exposure to similar conditions. Furthermore, an understanding of the influence of in-plane crystal growth, metal substitution, support type, and calcination method on oriented supported AFI films can have influence in other areas such as in catalysis, sensors, or host-guest assemblies.

2. Experimental

2.1 Preparation of $\text{AlPO}_4\text{-5}$ and CoAPO-5 powder and films

Aluminophosphate powder was prepared through hydrothermal growth using an aged precursor mixture with a composition of 1.0 Al_2O_3 : 1.3 P_2O_5 : *x* CoO : 1.2 TEA : 400 H_2O (denoted as A400) where *x* = 0 for $\text{AlPO}_4\text{-5}$ and *x* = 0.025 for CoAPO-5 . Aluminum isopropoxide (98%, Aldrich) was hydrolyzed in de-ionized (DI) water for 4.5

hr under stirring followed by the dropwise addition of phosphoric acid (85%, Aldrich). Following homogenization, the triethylamine (TEA, Aldrich) structure directing agent (SDA) was added dropwise and further allowed to homogenize. At this point, in the synthesis of CoAPO-5, cobalt (II) tetrahydrate (98%, Aldrich), was dissolved in a portion of the available water and added to the precursor solution, which was further allowed to age for 12 hr under stirring. The gel was added to Teflon liners, sealed in stainless steel autoclaves, and heated for 24 hr at 180 °C. At the time of completion, the autoclaves were quenched in cold water followed by centrifugation and drying.

Films were prepared hydrothermally on various supports in a conventional oven following seed deposition through an attachment-by-sonication procedure. The supports included 2.2 cm x 2.2 cm segments of glass (Normax), 2.0 cm x 2.0 cm segments of silicon (p-doped, Montco Silicon Technologies, Inc.), and home-made 22 mm diameter alumina supports. In each case, the substrates were cleaned and functionalized using a silane coupling agent, 3-chloropropyltrimethoxysilane (3-CPTMS). Next, the supports were subjected to sonication between two glass slides in an AlPO₄-5 or CoAPO-5 seed suspension in toluene under dry conditions. Seeds were previously synthesized with a molar composition of 1.0 Al₂O₃ : 1.3 P₂O₅ : x CoO : 1.2 TEA : 100 H₂O (denoted as A100) at 150 °C for 48 hr where x = 0 for AlPO₄-5 and x = 0.025 for CoAPO-5 and subsequently broken by sonication in dilute hydrochloric acid. For film formation, the supports were vertically aligned in Teflon liners and loaded in stainless steel autoclaves for hydrothermal seeded secondary growth at 150 °C for 10 hr. The secondary growth precursor solution was prepared from the A400 molar composition for both AlPO₄-5 and CoAPO-5. For tertiary hydrothermal growth, the A100 molar composition was used. The

solution was pre-crystallized with no support at 150 °C for 2 hr. At that time, the support which had undergone secondary growth was placed in the solution vertically within the liner and heated at 150 °C for 2 hr 50 min or 3 hr 10 min for AlPO₄-5 and CoAPO-5, respectively. At completion, the autoclave was quenched in room temperature water and the support was removed and carefully washed with DI water.

As-synthesized AlPO₄-5 and CoAPO-5 films on glass, silicon, and alumina supports were subjected to heat treatment through conventional calcination and/or rapid thermal processing to remove occluded SDA molecules. Conventional calcination was conducted with a heating ramp rate of 0.5 °C min⁻¹ to final temperatures in the range of 300 – 550 °C under flowing air. Rapid thermal processing (RTP) was completed using a Model E4-10 infrared chamber with a Model 915 controller (Research Inc.). Powder samples were placed on a silicon wafer and nominally heated within 60 sec to maximum temperatures in the range of 500 – 600 °C, held for 60 sec under flowing oxygen and subsequently cooled to room temperature with the assistance of a circulating cooling water jacket (ITW Cooling Systems) around the RTP chamber. Likewise, membranes on alumina supports were nominally heated at 800 °C min⁻¹ to maximum temperatures in the range of 400 – 700 °C, held for 60 sec under an oxygen flow, and cooled to room temperature.

2.2 Characterization

Microscopic features of the film morphology were observed using a JEOL 6700 and a JEOL JSM-7401F field-emission gun (FEG) scanning electron microscope (SEM) at typical conditions of 10 mA emission current and 5 kV operating voltage. A Thornley

Everhart lower secondary electron image (LEI) detector was used for topographical scans of the film surfaces. FTIR spectra were obtained from a Nicolet Series II Magna-IR System 750 with a diffuse reflectance accessory. Confirmation of preferred orientation and identification of aluminophosphate phase transitions were analyzed through diffraction patterns obtained on a Bruker AXS (Siemens) D5005 x-ray diffractometer (XRD) equipped with a 2.2 kW sealed copper source and a scintillation counter detector. Patterns were obtained in a 2θ range from $5 - 40^\circ$ with a step size of $0.05^\circ 2\theta$ and a dwell time of 1.0 sec. With diffractometer operation in $\theta/2\theta$ geometry, the back side of the film support was mounted on a designed holder to maintain a level surface during the goniometer rotation.

2.3 Membrane performance

A batch pervaporation system was designed to test the membrane quality following heat treatment. The membranes supported on porous $\alpha\text{-Al}_2\text{O}_3$ cylindrical discs were polished on the back side prior to the measurement. While enclosed tightly in a stainless steel module (with an available pervaporation surface area of $2.3 \times 10^{-4} \text{ m}^2$), the membrane was submerged in the hydrocarbon liquid feed consisting of a 50/50 mole percent mixture of n-heptane and 1,3,5-triisopropylbenzene (TIPB). A pitched blade propeller stationed above the module and a stir bar at the bottom of the vessel ensured good mixing near the membrane surface. A circulating water jacket was used to maintain a constant temperature during the measurements. Two condensers were used to collect the permeate upon establishing a vacuum. Pervaporation collection would continue up to 8 hr. At completion, the condenser was weighed to determine the total flux. The separation factor was

calculated as a ratio of the weight fractions of components in the permeate to the feed. A permeate sample was injected into an HP6890 gas chromatograph equipped with a flame ionization detector (FID). With an initial oven temperature of 40 °C, the temperature program for elution through the 0.25 μm DB-1 capillary column (J&W Scientific) was set at 25 °C min⁻¹ with a maximum temperature of 250 °C.

3. Results and Discussion

3.1 Early stages of in-plane AFI crystal growth

The secondary seeded growth technique was applied on porous α -Al₂O₃ supports for the synthesis of highly *c*-oriented columnar AlPO₄₋₅ crystals. We previously reported various conditions necessary to optimize crystalline intergrowth, orientation, and coverage through careful precursor mixture parameter variation [18], although the aforementioned experiments were conducted on dense silicon substrates. Figure 1(a) shows the SEM image following secondary growth on a home-made α -Al₂O₃ support using a dilute A400 precursor molar composition (see Experimental Section 2.1). The crystals exhibited a columnar morphology with the elongated pore channel *c*-axis aligned perpendicularly to the support surface. Tertiary, in-plane growth was subsequently completed in order to improve intergrowth between supported crystals without reducing the degree of preferred orientation, as seen in Figure 1(b). The cross-sectional images in Figure 1(c) and 1(d) demonstrate the interwoven network of crystal domains following tertiary growth.

The mechanism of intergrowth of the secondary columnar crystals upon tertiary treatment is based upon the formation of a network of flake-like crystal domains that are preferentially grown in a direction parallel to the support, as seen in the SEM images of

Figure 2. Growth direction and crystal morphology are dependent upon dilution of the precursor species under the same reaction conditions. Specifically, dilute A400 precursor mixtures favor growth along the channel direction yielding columnar crystals, while dense ones (A100) produce flake-like grains due to preferred growth perpendicular to the channels. With respect to the support surface, secondary treatment using dilute A400 mixtures favors *c*-out-of-plane growth of columnar crystals that are oriented perpendicular to the support (Figure 1(a)), while by shifting to dense A100 mixtures upon tertiary treatment, the growth direction is turned to in-plane, thus inducing intergrowth (Figure 1(b)). Despite the fact that the growth direction changes, the channel orientation of the tertiary domains remains perpendicular to the support due to the fact that the flake-like grains are nucleated on the sides of the originally *c*-oriented mother columnar crystals thus following the same orientation. Consequently, due to the dominant growth direction during tertiary treatment being parallel to the support and perpendicular to the columnar crystals, an additional growth step does not cause any considerable increase in the thickness of the film, as also demonstrated in our previous study using dense substrates [17]. Figures 2(a) and 2(b) correspond to early stages of in-plane growth in powder samples, confirming that nucleation of flake-like domains takes place on the side surfaces of the original columnar crystals. As growth progresses, the crystals are expanded from the face of the columnar parent and dominate the outer faces (Figures 2(c) and (d)). At the final stage of film formation, grains grown from neighboring columnar crystals are merged with each other creating a well-intergrown network, as shown in the cross sectional images of Figures 1(c) and (d), which correspond to a tertiary growth duration of 2 h 50 min.

3.2 Heat treatment of AFI powders and membranes

As previously mentioned, there have been reports of thermal instability regarding aluminophosphate-type materials. Such behavior could create problems for applications as molecular sieving membranes or catalytic hosts. Preliminary experiments were conducted using CoAPO-5 powder, a cobalt-substituted $\text{AlPO}_4\text{-5}$ variant. Figure 3(a) shows the XRD pattern for the characteristically blue as-synthesized powder. Two methods of calcination were employed to study the effect of thermal treatment on the microporous material. First, conventional calcination (CC), with a maximum temperature of 400 °C (Figure 3(b)) or 550 °C (Figure 3(c)), was conducted with a ramping rate of 0.5 °C min⁻¹ and held for 10 hr in flowing air. As reported elsewhere [30], the AFI material undergoes a unit cell volume expansion of +3.0% based on the hexagonal crystal system. Here, an expansion was observed along the *a*-axis (+1.9%) while a contraction was observed along the *c*-axis (-0.76%), which are related to opening of the pores from removal of the SDA molecules occluded in the framework. Furthermore, rapid thermal processing (RTP) was used as a faster means by which to remove the SDA molecules. The crystalline powder was nominally heated to 500 °C (Figure 3(d)) or 600 °C (Figure 3(e)) within 60 sec and held at that temperature for 60 sec under an oxygen flow to accelerate combustion of the SDA. Along with retaining crystallinity and the inherent AFI framework, the unit cell behavior following RTP was similar to that of the CC case with a reduction in calcination time of nearly 45 hr.

Initial membrane calcination experiments were focused on $\alpha\text{-Al}_2\text{O}_3$ supported $\text{AlPO}_4\text{-5}$ columnar crystals following secondary or tertiary growth. In Figure 4(a), we found that following conventional calcination at 400 °C, the supported crystals from

secondary growth tolerated the high temperature and retained the original AFI framework. However, applying the same calcination conditions to a film following tertiary growth resulted in the formation of a densified aluminophosphate tridymite form (AlPO_4 -tridymite). The fact that purely columnar, non-intergrown films are more resistant to high temperature treatment than intergrown films consisting of both columnar and flake-like grains indicates that film stability is morphology-dependent. Figure 4(b) is a representative SEM image following the calcination of a tertiary AlPO_4 -5 membrane, which shows abundant surface defects combined with crystal densification. From Figure 4(c), conventional calcination of a metal-substituted CoAPO-5 leads to the formation of AlPO_4 -tridymite with visible crystal surface defects.

3.3 Influence of support type

A series of experiments were performed to determine any impact the substrate may have on the phase of the supported crystals in order to find the optimal processing conditions that would yield functional AFI-type films for various applications. As previously noted, the secondary growth of seeded alumina supports exhibited superior thermal stability when compared to films which were exposed to tertiary growth. Figure 5 shows XRD patterns of films subjected to 300 °C, 350 °C, 400 °C, and 550 °C for the removal of SDA molecules through conventional calcination (CC). The as-synthesized membrane (Figure 5(a)) and after heating to 300 °C (Figure 5(b)) resulted in no observable AlPO_4 -tridymite. However, as seen in the powder samples, at temperatures as low as 300 °C, the material does undergo a unit cell volume expansion with a shift in the (100) and (002) peaks relative to the as-synthesized material. According to the pattern in Figure

5(c), the appearance of AlPO_4 -tridymite occurred at temperatures as high as 350 °C, resulting in a mixture of densified and microporous material. After calcination at 400 °C (Figure 5(d)), the phase is predominantly AlPO_4 -tridymite, indicating a nearly complete loss of the ordered AFI framework structure. A silica coating was applied by a slip-coating procedure to the surface of the support considering that direct contact of the AFI crystals with the $\alpha\text{-Al}_2\text{O}_3$ substrate could be impacting stability at elevated temperatures. Figure 5(e) shows that while an oriented film could be synthesized on porous silica, an intermediate layer between the alumina support and the crystals could not prevent destabilization at thermal processing conditions.

Films were grown on dense supports in order to investigate the phase dependence on substrate type when subjected to calcination temperatures. Figure 6 shows the XRD patterns for the as-synthesized and heat-treated films of *c*-oriented AlPO_4 -5 following tertiary growth on glass substrates. Figure 6(a) indicates that the as-grown film is crystalline and highly oriented based on the dominance of the representative (002) peak at a 2θ of 20.9°. Figures 6(b) and 6(c) show that the film remained crystalline and highly oriented while treated for 10 hr at 300 °C and 400 °C, respectively. It can also be seen that the AFI framework is retained at temperatures up to 400 °C. From Figure 6(d), at 500 °C a mixture of AFI and AlPO_4 -tridymite phases can be observed. Although phase transformation was not entirely avoided, it was delayed nearly 150 °C when compared to the porous alumina support case, demonstrating that structural stability is also support-dependent.

Next, dense silicon supports were examined using oriented CoAPO -5 films. Preferred orientation of an as-grown film was confirmed in Figure 7(a). Similarly to the

porous alumina and glass substrate cases, following CC at 300 °C (Figure 7(b)) the AFI structure was retained with high orientation and crystallinity. Moreover, at 550 °C with CC conditions, there was no observable presence of an AlPO_4 -tridymite phase, in contrast to alumina and glass supports cases that both resulted in densification upon the same calcination conditions. Although the exact mechanism for crystal destabilization and how it is dependent upon the type of support are not known at this time, it is concluded that the order of crystalline stability based on support type for columnar AFI-type films when subjected to CC is silicon > glass > porous alumina.

3.4 Template removal through rapid thermal processing

Rapid thermal processing (RTP) was used as an alternative calcination technique for removing SDA molecules occluded in AlPO_4 -5 membranes on $\alpha\text{-Al}_2\text{O}_3$ supports. There have been many reports on the debilitating crack formation in silicalite-1 (zeolite type MFI) membranes as a result of SDA removal [31-34] as well as techniques proven to overcome such limitations [35-36]. The implementation of RTP improved the quality of the MFI films by reducing the formation of debilitating grain boundary defects.

Here, RTP was used in order to quickly evacuate the pore channels of remnant SDA molecules through fast combustion before densification with a loss in microporosity. Figure 8 shows the diffraction patterns with the corresponding morphology of RTP-treated membranes subjected to various maximum temperatures with the as-synthesized membrane pattern present for comparison (Figure 8(a)). From Figure 8(b), the AFI framework stability is retained upon RTP at a maximum temperature of 400 °C. The morphology remained intact with few observable crystalline defects. However, increasing

the hold temperature to 500 °C resulted in a mixture of AlPO₄-5 and AlPO₄-tridymite based on the diffraction pattern in Figure 8(c). More substantial crystalline defects were present with crystal densification. Figure 8(d) indicates that the membrane underwent complete transformation to AlPO₄-tridymite with a resultant morphology identical to that obtained following conventional calcination at 550 °C sustained for 10 hr. The XRD pattern peak shifts from an RTP maximum temperature of 400 °C related to the as-synthesized membrane resulted in an *a*-axis expansion (+1.1%) and *c*-axis contraction (-0.63%), in a similar manner to the XRD pattern analyzed in the powder form.

Choi et al. reported using CC after RTP in order to fully remove SDA molecules from the MFI pore network [35]. However, in our case, further CC resulted in the formation of AlPO₄-tridymite. By comparing the XRD patterns from a hold temperature of 400 °C in Figure 5(d) (CC) to Figure 8(b) (RTP), the dwell time appeared to have an impact on the degree of densification, indicating that RTP may quickly evacuate the channels prior to framework destabilization. FTIR spectra in Figure 9 emphasize amine decomposition following RTP. In Figure 9(a), the representative spectrum of an as-synthesized AlPO₄-5 membrane on porous α -Al₂O₃ shows the lattice framework vibrations along with triethylamine SDA peaks, which may be observed in the 1400 – 1500 cm⁻¹ and 2800 – 3000 cm⁻¹ regions [37]. As can be seen from Figure 9(b), based on the absence of the aforementioned SDA region peaks, RTP with a maximum holding temperature of 400 °C decomposed the occluded amine molecules prior to significant structure alteration (Figure 8(b)). Given that membranes produced from secondary growth are stable following CC while those from tertiary growth have structure limitations during

either CC or RTP, it may be concluded that the degree of intergrowth affects the phase transformation kinetics.

3.5 Measuring membrane quality through pervaporation

AFI-type membranes can be used as a molecular sieve through the selection of molecules close to the diameter of the pore channel (0.73 nm) [4,14], yet there are no up-to-date studies investigating the separation capabilities of AFI-type membranes that exhibit structural homogeneity, crystalline intergrowth, and preferred orientation throughout the extent of the membrane. We have conducted pervaporation measurements using a 50/50 mole percent feed solution of n-heptane (kinetic diameter 0.43 nm) and 1,3,5-triisopropylbenzene (TIPB, 0.85 nm) to investigate the quality of CC and RTP-treated $\text{AlPO}_4\text{-5}$ membranes. Figure 10(a) and (b) show the total flux and separation factors through the calcined membranes, respectively. As expected, the CC membrane exhibited a high flux but with an associated separation factor close to 1, which is attributed to the loss of the AFI microstructure and defect generation during post-synthetic heat treatment.

Applying RTP (nominal ramp rate of $800\text{ }^\circ\text{C min}^{-1}$ to a maximum of $400\text{ }^\circ\text{C}$, held for 60 sec, and cooled to room temperature) to an as-synthesized membrane imparted an improvement in the separation factor (approximately 3) with an order of magnitude decrease in the total flux. The corresponding XRD pattern from Figure 8(b) showed the slight appearance of a representative $\text{AlPO}_4\text{-tridymite}$ peak, which may contribute to a decrease in sieving capability. As a function of liquid feed temperature, the separation factor decreased with a corresponding flux increase. It is evident that the columnar *c*-oriented AFI membranes are not promising for molecular separations.

4. Conclusions

Highly *c*-oriented, intergrown, continuous crystalline aluminophosphate AlPO₄-5 and CoAPO-5 (both of the AFI framework type) were grown on porous α -Al₂O₃ supports by the seeded growth method. By varying the crystallization duration time, a mechanism for in-plane, flake-like crystal nucleation during tertiary growth was revealed. While the AFI powder form presented a typical unit cell volume expansion (with *a*-axis expansion and *c*-axis contraction) when exposed to either CC or RTP conditions, the oriented film displayed instability at high temperatures. Films from secondary growth did not display such behavior, indicating that intergrowth affects the phase transformation behavior. Analysis by varying the support type revealed that the films grown on dense substrates (silicon, glass) had a higher degree of stability than ones on porous alumina. RTP overcame structural deficiencies through fast template combustion while retaining AFI microstructure characteristics at temperatures sufficient to remove the occluded SDA molecules from the pores by limiting thermal exposure time. However, pervaporation measurements did not indicate satisfactory membrane separation performance (separation factor of 2.8 with a corresponding flux of 1.2 kg m⁻² hr⁻¹ for a liquid feed of n-heptane/1,3,5-triisopropylbenzene), indicating that alternative growth methods and microstructures should be investigated.

Acknowledgements

Support by the American Chemical Society (ACS-PRF) and the European Community through the FP7 NextGTL project and a Marie Curie International Reintegration Grant

(FP7, grant agreement no. 210947) is greatly appreciated. Parts of this work were carried out in the Characterization Facility on the campus of the University of Minnesota-Twin Cities, which receives partial support from NSF through the MRSEC program.

References

- [1] J. Caro, M. Noack, *Microporous Mesoporous Mater.* 115 (2008) 215-233.
- [2] M.E. Davis, *Nature* 417 (2002) 813-821.
- [3] M.A. Snyder, M. Tsapatsis, *Angew. Chem., Int. Ed.* 46 (2007) 7560-7573.
- [4] M. Noack, P. Kolsch, D. Venzke, P. Toussaint, J. Caro, *Microporous Mater.* 3 (1994) 201-206.
- [5] V. Kukla, J. Kornatowski, D. Demuth, I. Girnus, H. Pfeifer, L.V.C. Rees, S. Schunk, K.K. Unger, J. Karger, *Science* 272 (1996) 702-704.
- [6] S. Feng, T. Bein, *Science* 265 (1994) 1839-1841.
- [7] R. Xu, G. Zhu, X. Yin, X. Wan, S. Qiu, *Microporous Mesoporous Mater.* 90 (2006) 39-44.
- [8] J.-C. Lin, M.Z. Yates, *Chem. Mater.* 18 (2006) 4137-4141.
- [9] T. Munoz, K.J. Balkus, *Chem. Mater.* 10 (1998) 4114-4122.
- [10] R. Xu, G. Zhu, X. Yin, X. Wan, S. Qiu, *J. Mater. Chem.* 16 (2006) 2200-2204.
- [11] T.-G. Tsai, H.-C. Shih, S.-J. Liao, K.-J. Chao, *Microporous Mesoporous Mater.* 22 (1998) 333-341.
- [12] L. Campbell, T. Kemmitt, M. Bowden, A. Kirchner, *Curr. Appl. Phys.* 8 (2008) 479-481.

- [13] E. Hu, Y.L.W. Huang, Q. Yan, D. Liu, Z. Lai, *Microporous Mesoporous Mater.* 126 (2009) 81-86.
- [14] W. Yang, B. Zhang, X. Liu, *Microporous Mesoporous Mater.* 117 (2009) 391-394.
- [15] W. Yang, X. Liu, L. Zhang, B. Zhang, *Langmuir* 25 (2009) 2271-2277.
- [16] G.N. Karanikolos, J.W. Wydra, J.A. Stoeger, H. Garcia, A. Corma, M. Tsapatsis, *Chem. Mater.* 19 (2007) 792-797.
- [17] G.N. Karanikolos, H. Garcia, A. Corma, M. Tsapatsis, *Microporous Mesoporous Mater.* 115 (2008) 11-22.
- [18] C.M. Veziri, M. Palomino, G.N. Karanikolos, A. Corma, N.K. Kanellopoulos, M. Tsapatsis, *Chem. Mater.* 22 (2010) 1492-1502.
- [19] F.Y. Jiang, J.P. Zhai, J.T. Ye, J.R. Han, Z.K. Tang, *J. Cryst. Growth* 283 (2005) 108-114.
- [20] K.-H. Schnabel, G. Finger, J. Kornatowski, E. Löffler, C. Peuker, W. Pilz, *Microporous Mater.* 11 (1997) 293-302.
- [21] Y. Hu, A. Navrotsky, C.-Y. Chen, M.E. Davis, *Chem. Mater.* 7 (1995) 1816-1823.
- [22] J.O. Perez, R.B. Borade, A. Clearfield, *J. Mol. Struct.* 470 (1998) 221-228.
- [23] X.S. Zhao, G.Q. Lu, *Microporous Mesoporous Mater.* 44-45 (2001) 185-194.
- [24] V.P. Shiralkar, C.H. Saldarriaga, J.O. Perez, A. Clearfield, M. Chen, R.G. Anthony, J.A. Donohue, *Zeolites* 9 (1989) 474-482.
- [25] U. Lohse, R. Bertram, K. Jancke, I. Kurzwaski, B. Parlitz, E. Löffler, E. Schreier, *J. Chem. Soc. Faraday Trans.* 91 (1995) 1163-1172.
- [26] H.P. Rao, M.A. Zanjanchi, P. Massiani, D. Barthomeuf, S. Launay, A. Davidson, M. Che, *Res. Chem. Intermed.* 25 (1999) 57-75.

- [27] H.-X. Li, M.E. Davis, *J. Chem. Soc. Faraday Trans.* 89 (1993) 957-964.
- [28] W. Schmidt, F. Schuth, H. Reichert, K. Unger, B. Zibrowius, *Zeolites* 12 (1992) 2-8.
- [29] K. Sorby, R. Szostak, J.G. Ulan, R. Gronsky, *Catal. Lett.* 6 (1990) 209-214.
- [30] J.W. Richardson, J.J. Pluth, J.V. Smith, *Acta Crystallogr.* C43 (1987) 1469-1472.
- [31] G. Xomeritakis, Z. Lai, M. Tsapatsis, *Ind. Eng. Chem. Res.* 40 (2001) 544-552.
- [32] J. Dong, Y.S. Lin, M.Z.-C. Hu, R.A. Peascoe, E.A. Payzant, *Microporous Mesoporous Mater.* 34 (2000) 241-253.
- [33] M.L. Gualtieri, C. Andersson, F. Jareman, J. Hedlund, A.F. Gualtieri, M. Leoni, C. Meneghini, *J. Membr. Sci.* 290 (2007) 95-104.
- [34] H.-K. Jeong, Z. Lai, M. Tsapatsis, J.C. Hanson, *Microporous Mesoporous Mater.* 84 (2005) 332-337.
- [35] J. Choi, H.-K. Jeong, M.A. Snyder, J.A. Stoeger, R.I. Masel, M. Tsapatsis, *Science* 325 (2009) 590-593.
- [36] W.C. Yoo, J.A. Stoeger, P.-S. Lee, M. Tsapatsis, A. Stein, *Angew. Chem., Int. Ed.* 122 (2010) 8881-8885.
- [37] G. Muller, J. Bodis, G. Eder-Mirth, J. Kornatowski, J.A. Lercher, *J. Mol. Struct.* 410-411 (1997) 173-178.

Figure Captions

Figure 1. SEM images of $\text{AlPO}_4\text{-5}$ growth on a seeded porous $\alpha\text{-Al}_2\text{O}_3$ support following (a) secondary growth and (b) tertiary growth. Cross-sectional SEM images reveal (c) an interwoven network of crystalline domains and (d) an area of the interwoven network at higher resolution of the final tertiary-grown membranes.

Figure 2. SEM images highlighting the evolution of flake-like crystals during early stages of tertiary, in-plane growth.

Figure 3. XRD patterns of CoAPO-5 powder subjected to various thermal treatments.

The (a) as-synthesized powder was exposed to conventional calcination at (b) 400 °C and (c) 550 °C and RTP at (d) 500 °C and (e) 600 °C.

Figure 4. (a) XRD pattern of an AlPO₄-5 membrane on porous α -Al₂O₃ after conventional calcination at 400 °C following (top) secondary growth and (bottom) tertiary growth.

SEM images reveal structural defects after conventional calcination in tertiary (b) AlPO₄-5 and (c) CoAPO-5 membranes.

Figure 5. XRD patterns showing the densification development of (a) AlPO₄-5

membranes on porous α -Al₂O₃ supports after conventional calcination at (b) 300 °C, (c) 350 °C, (d) 400 °C, and (e) 550 °C with a silica intermediate layer.

Figure 6. XRD pattern of an AlPO₄-5 film on glass (a) as-grown, and followed by conventional calcination at (b) 300 °C, (c) 400 °C, and (d) 500 °C.

Figure 7. XRD pattern of a CoAPO-5 film on silicon (a) as-grown, and followed by conventional calcination at (b) 300 °C, and (c) 550 °C.

Figure 8. XRD pattern of an AlPO₄-5 membrane on a porous α -Al₂O₃ support (a) as-grown and followed by RTP at (b) 400 °C, (c) 500 °C, and (d) 600 °C with corresponding SEM images.

Figure 9. FTIR spectra of an AlPO₄-5 membrane on a porous α -Al₂O₃ support (a) as-grown and (b) following RTP at 400 °C.

Figure 10. Effect of pervaporation module temperature on the (a) flux and (b) separation factor of CC- or RTP-treated $\text{AlPO}_4\text{-5}$ membranes on porous $\alpha\text{-Al}_2\text{O}_3$ supports from an equimolar liquid feed consisting of n-heptane and 1,3,5-triisopropylbenzene.

Figure 1.

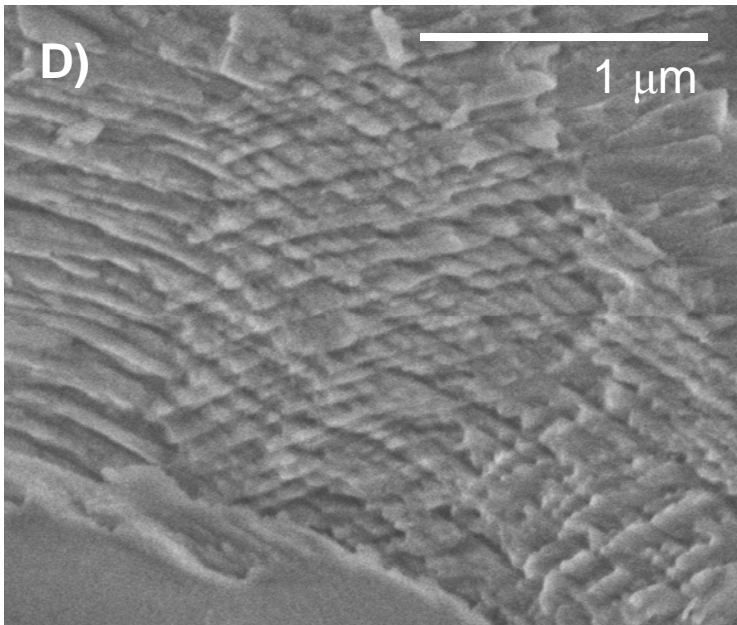
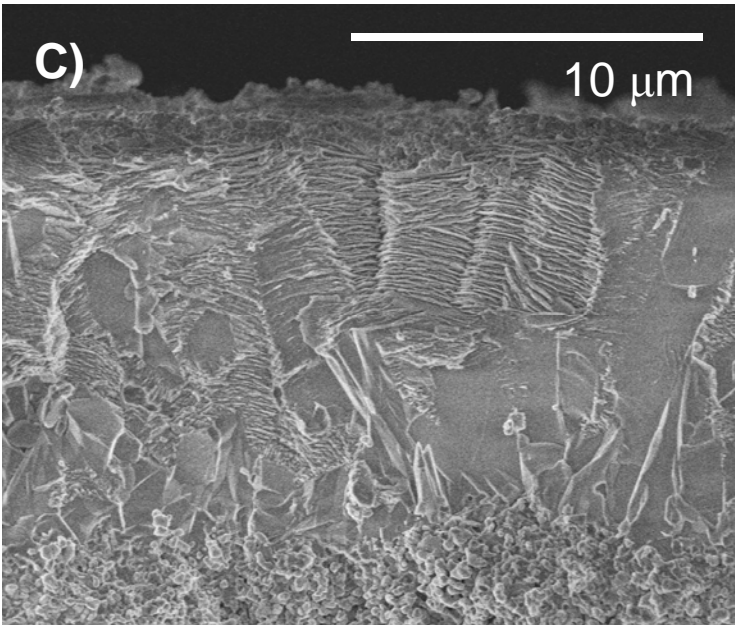
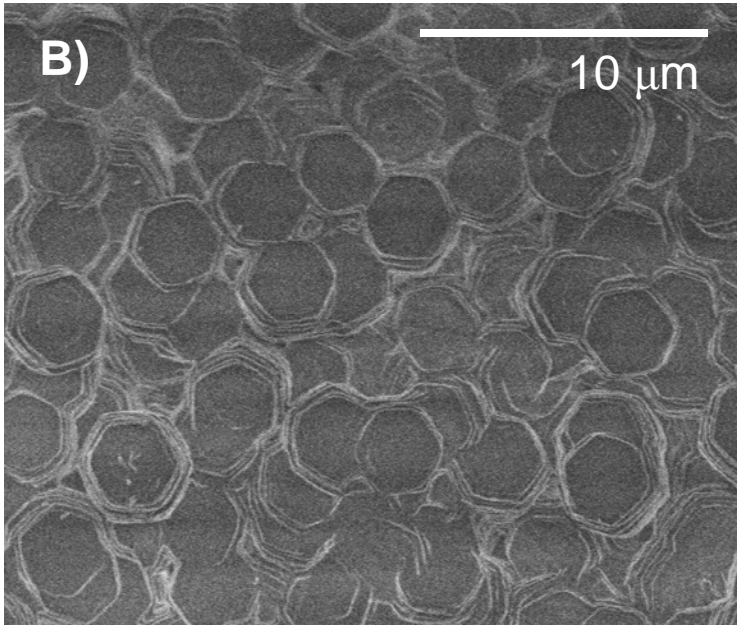
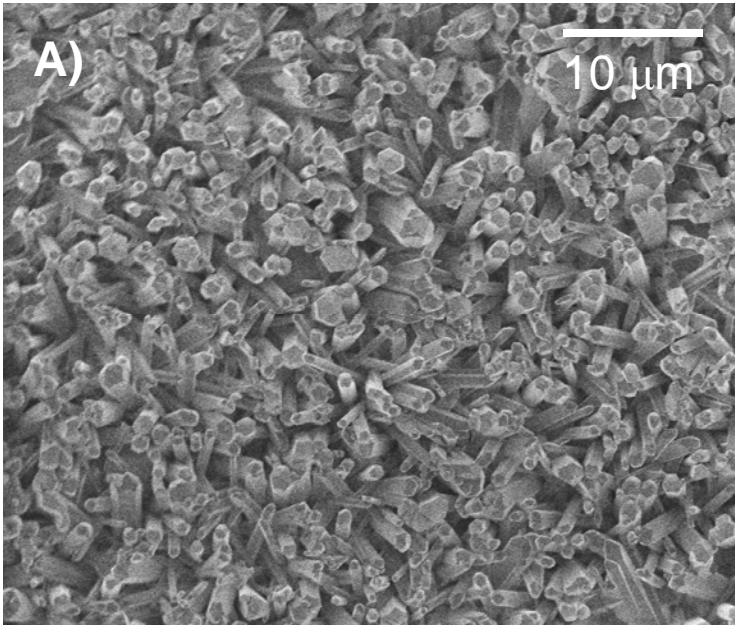


Figure 2.

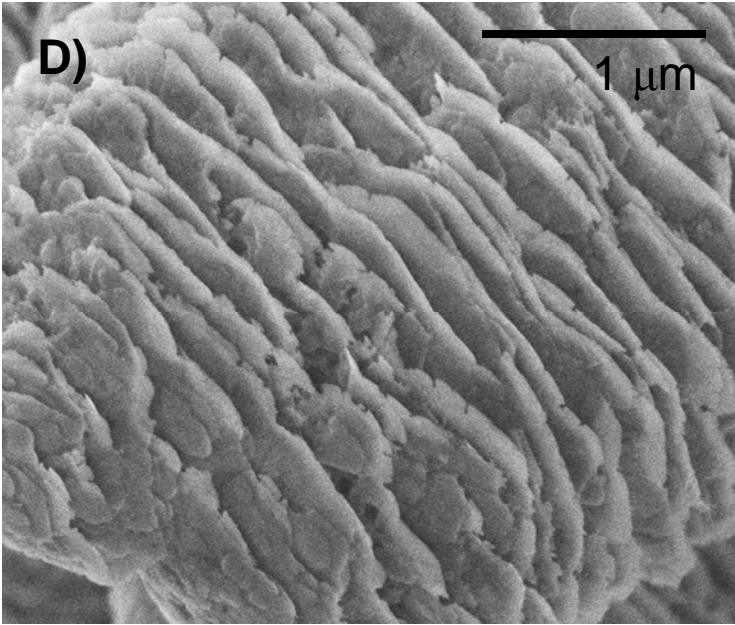
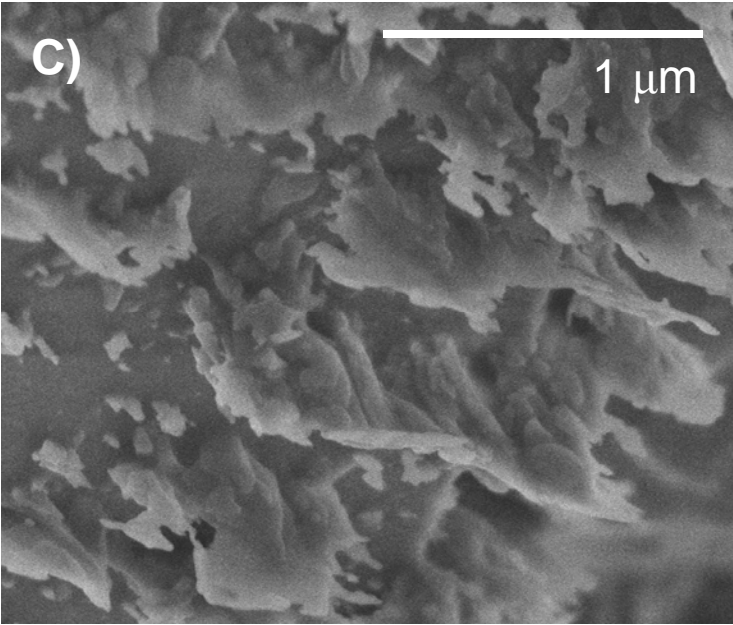
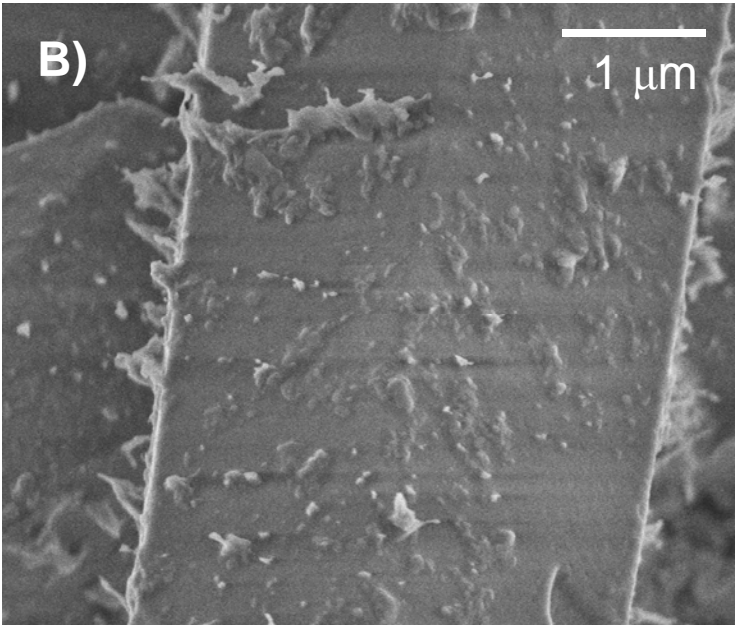
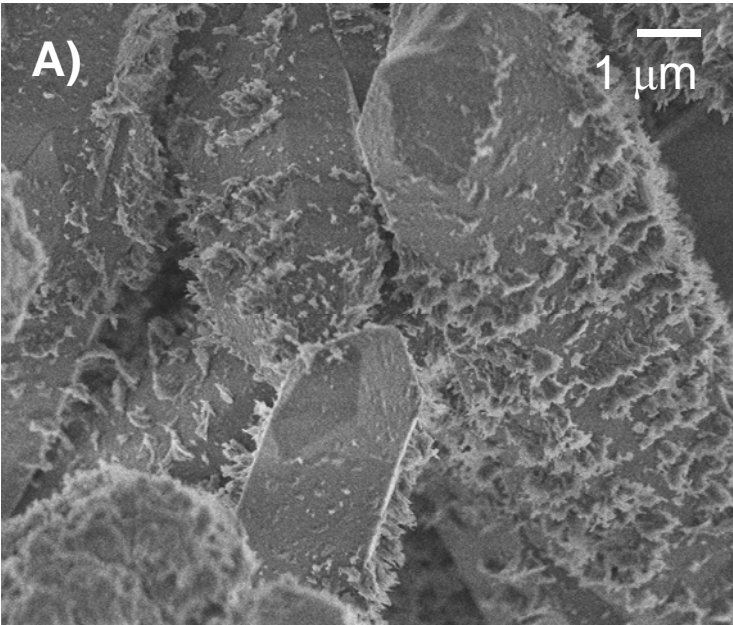


Figure 3.

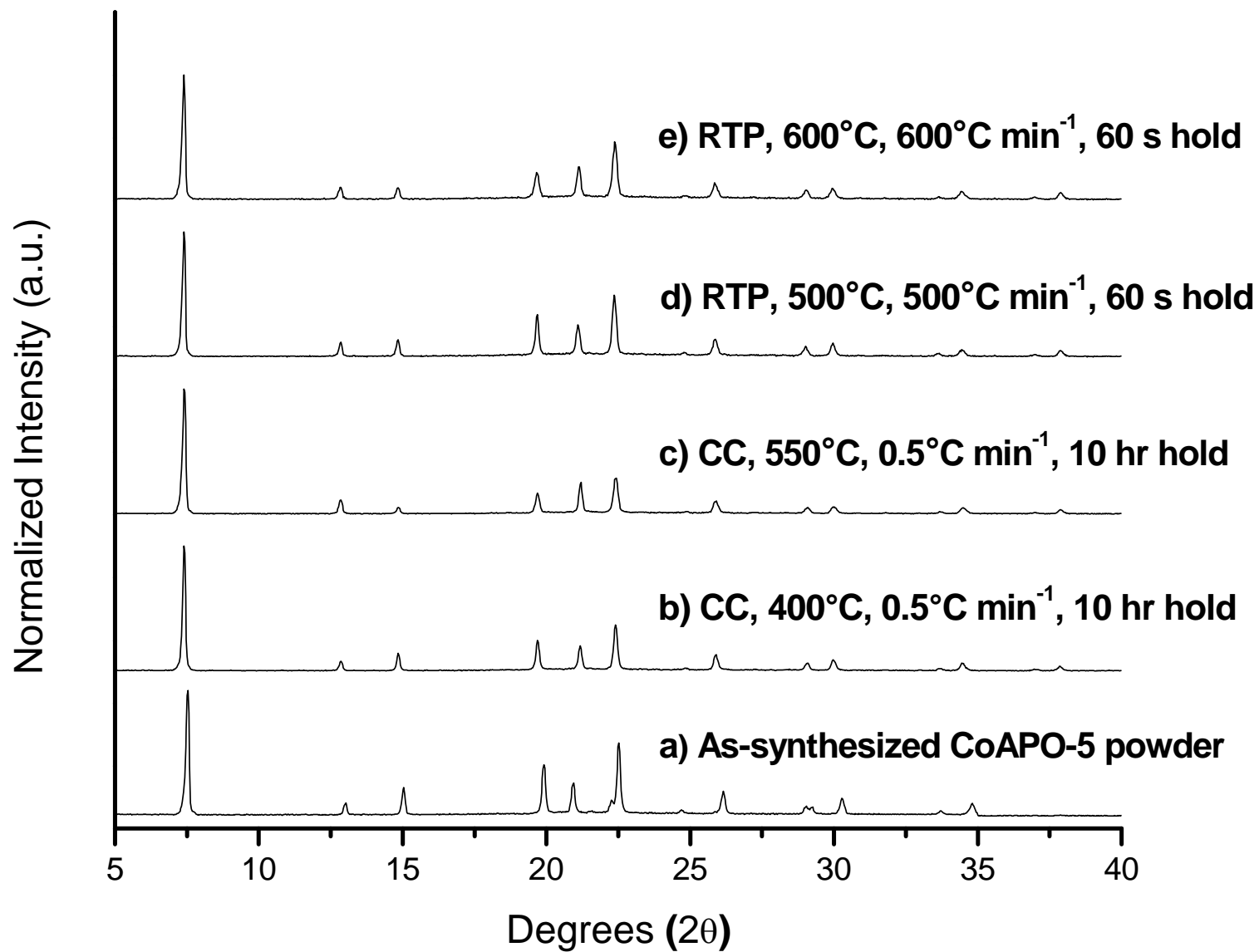


Figure 4.

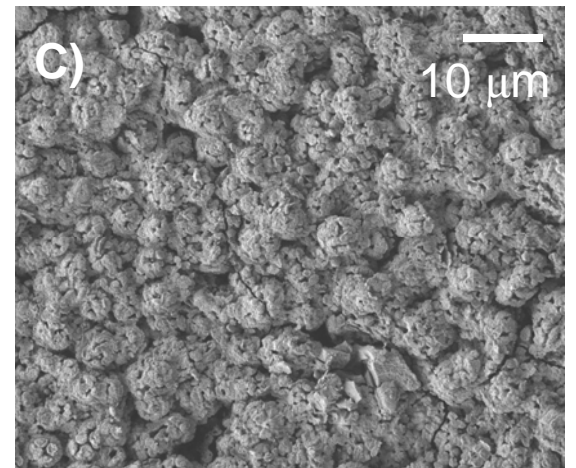
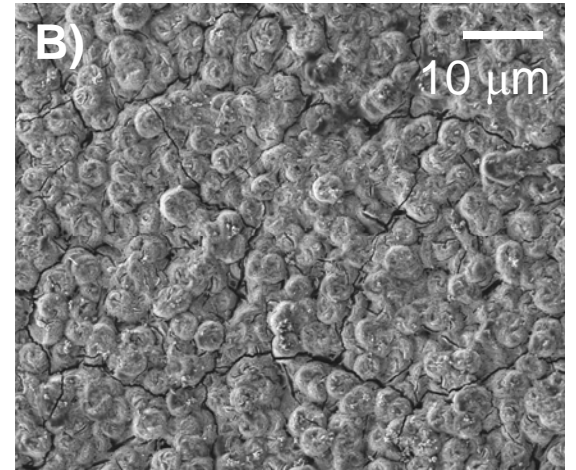
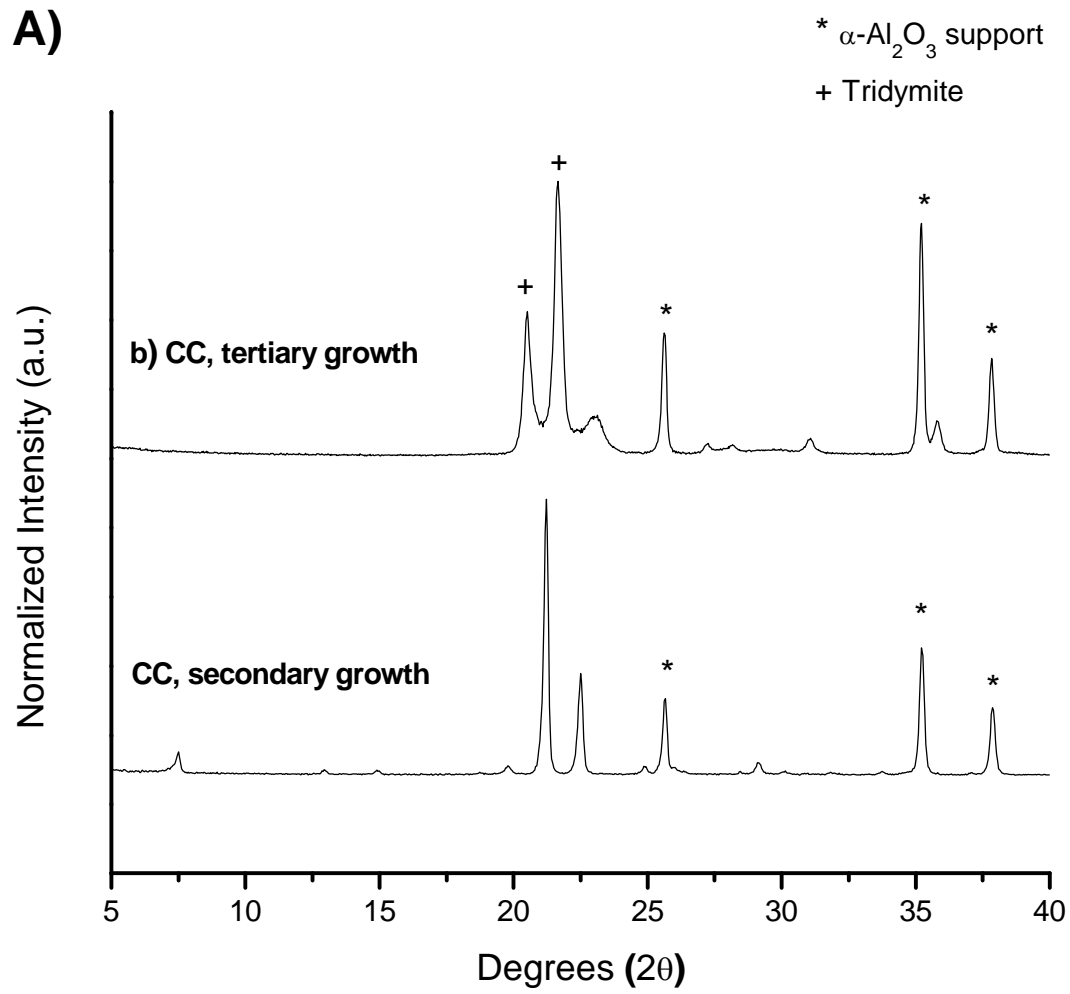


Figure 5.

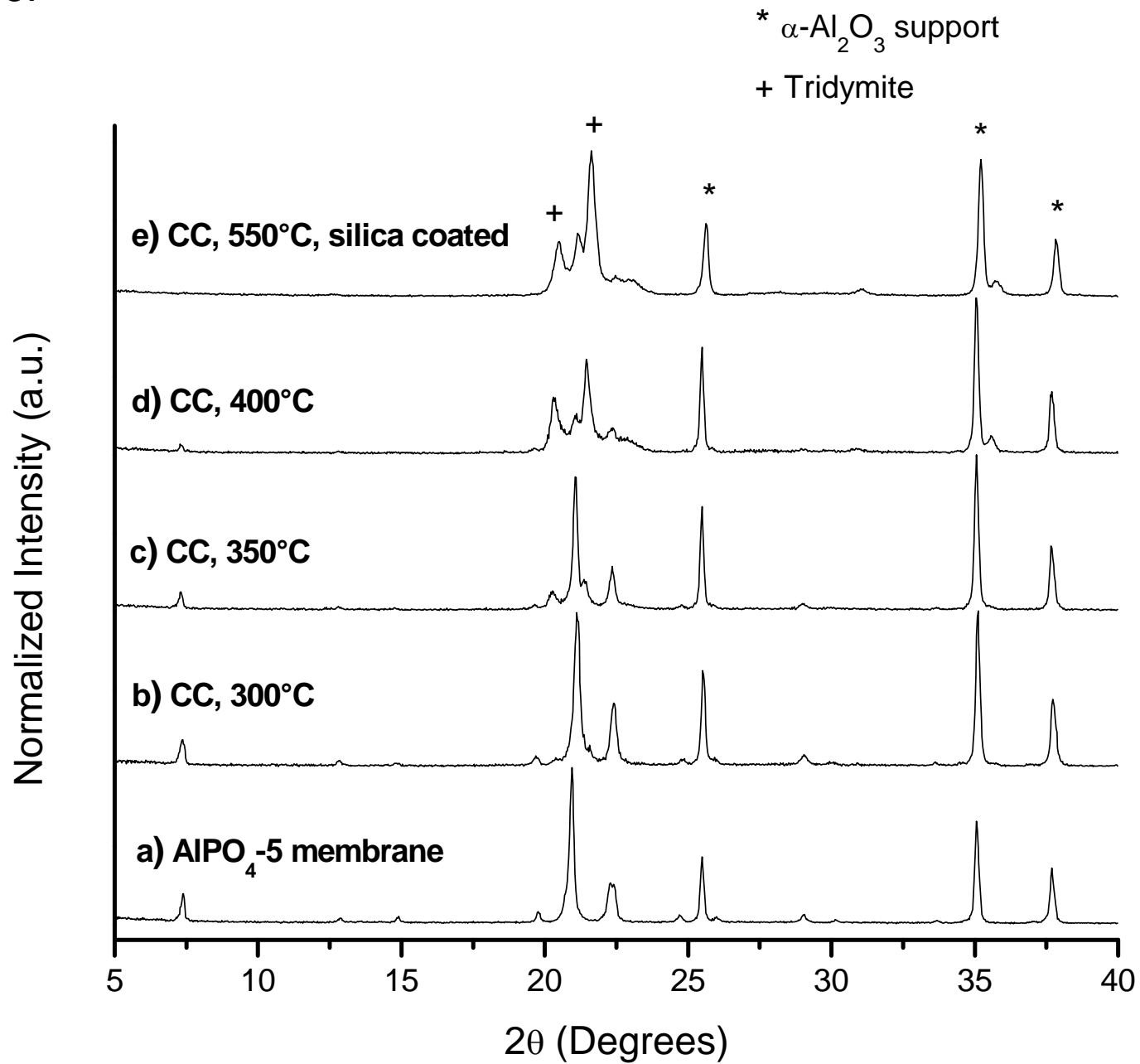


Figure 6.

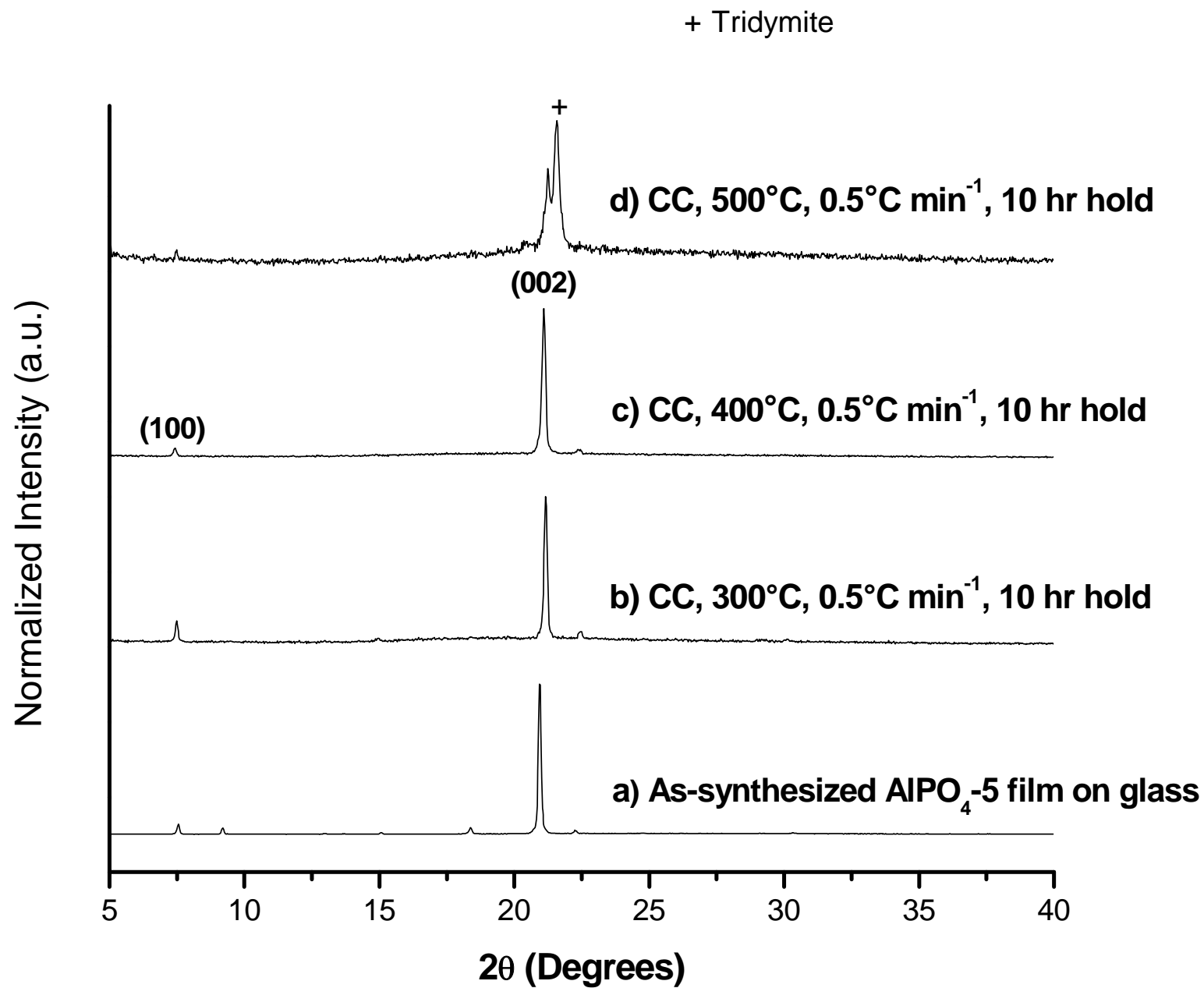


Figure 7.

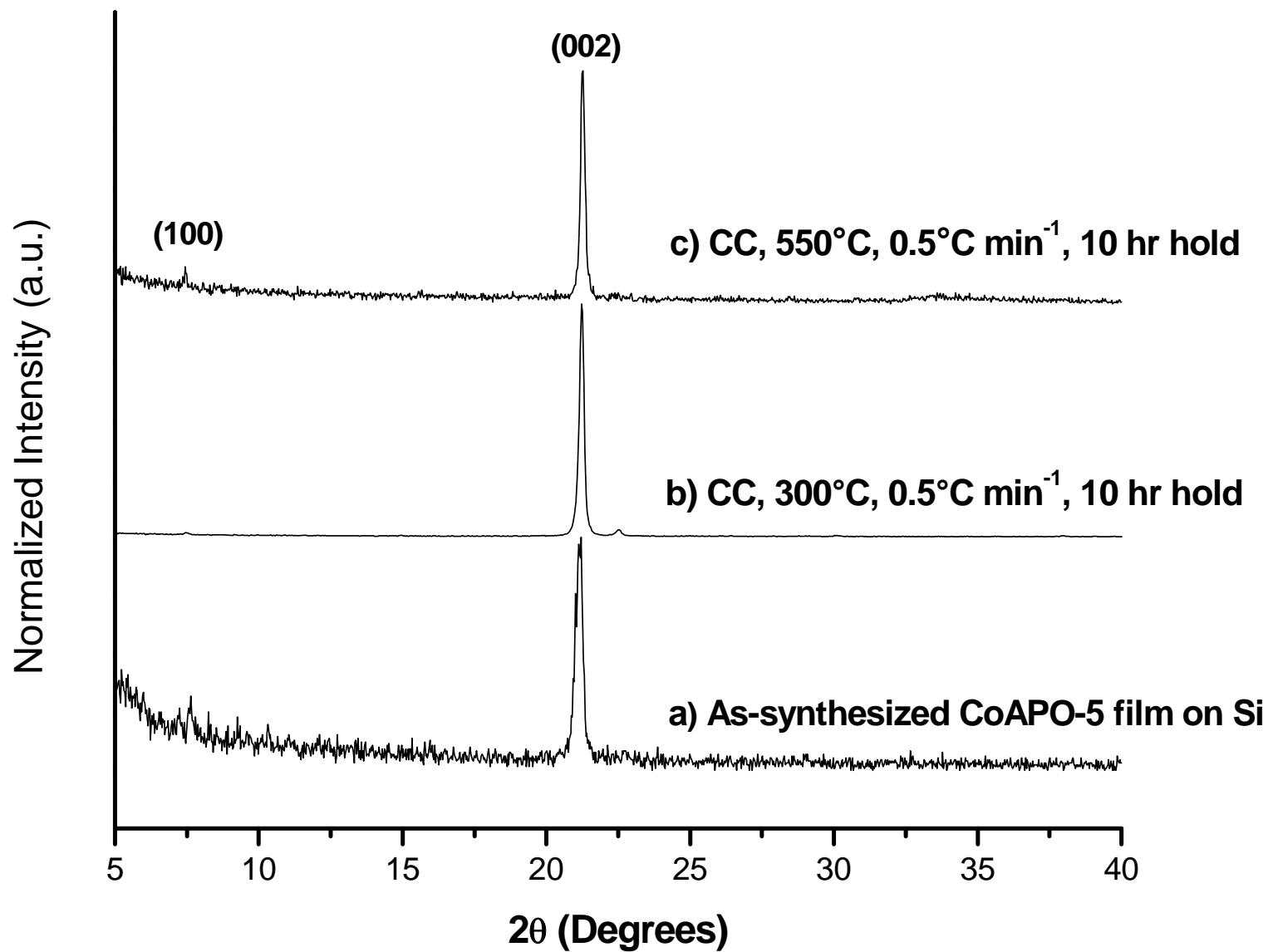


Figure 8.

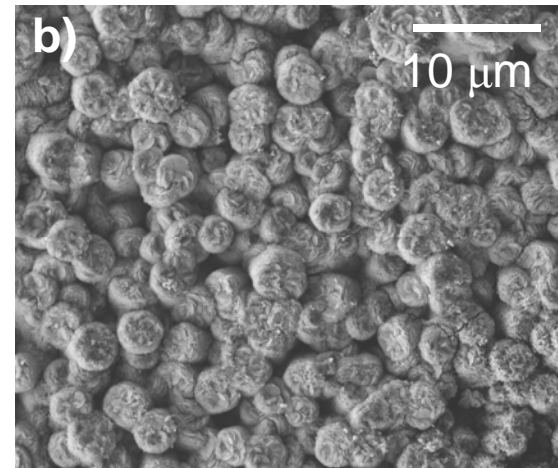
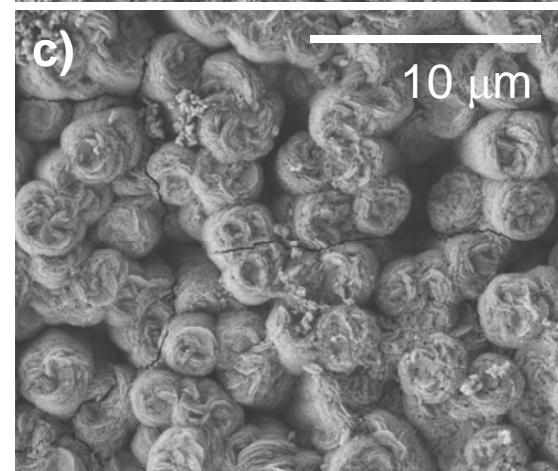
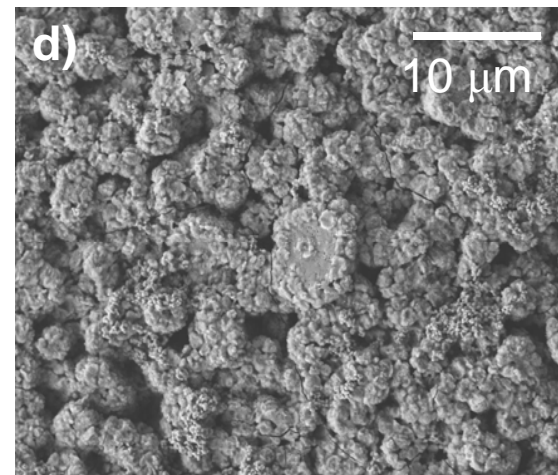
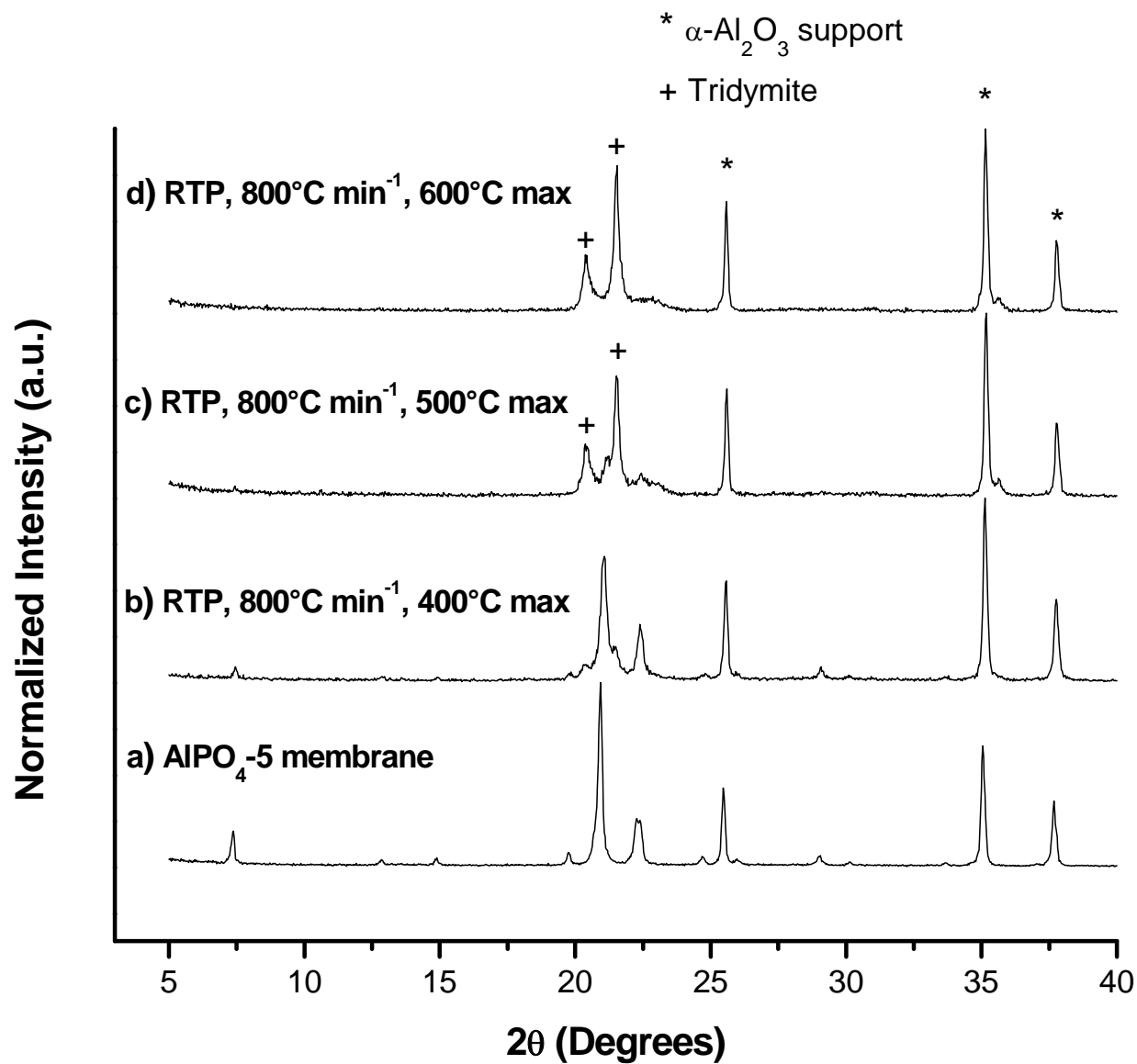


Figure 9.

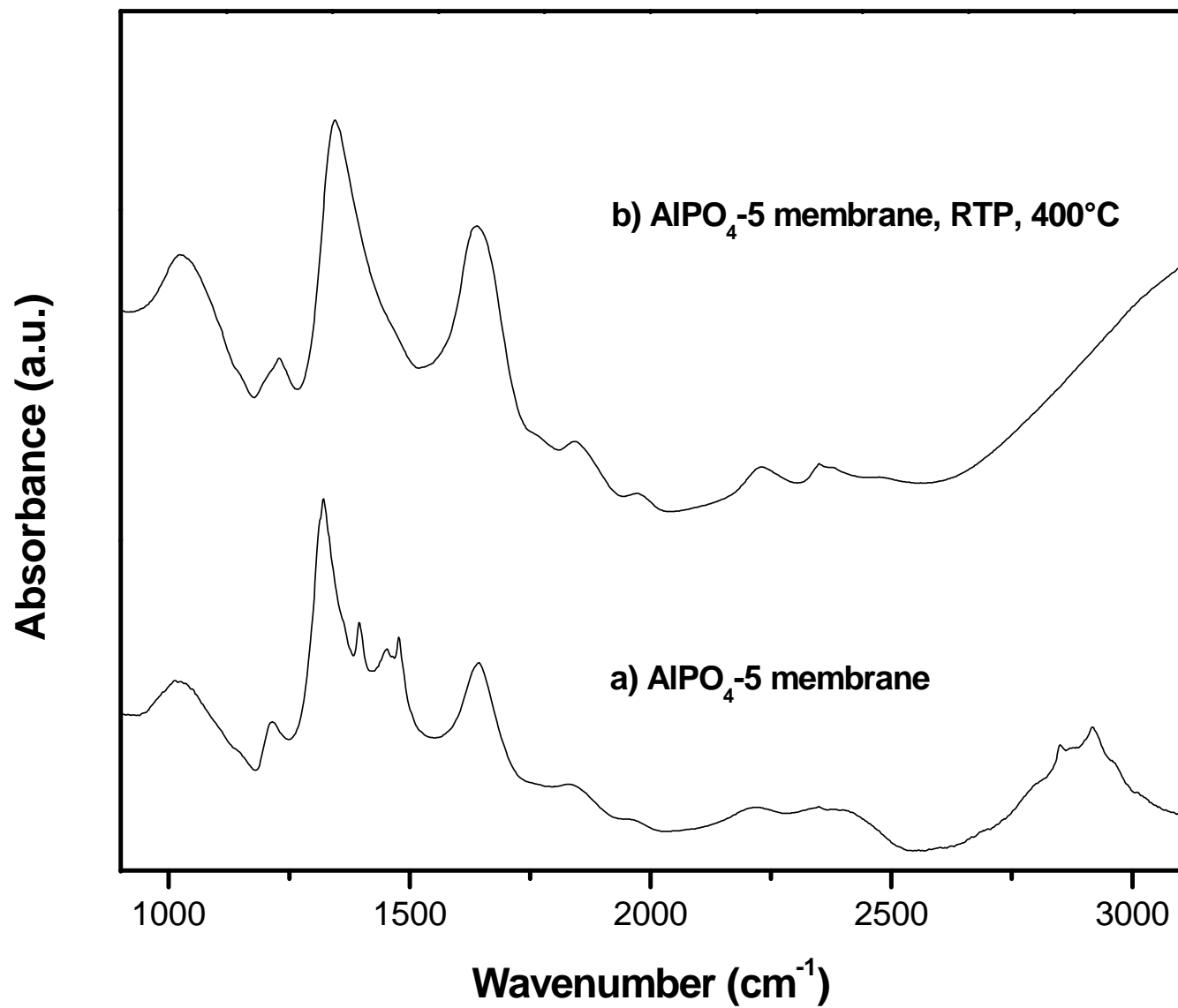


Figure 10.

